View metadata, citation and similar papers at core.ac.uk

brought to you by CORE

provided by Elsevier - Publisher Connector

Water Resources and Industry 4 (2013) 32–50

Contents lists available at ScienceDirect

Water Resources and Industry

journal homepage: www.elsevier.com/locate/wri

Application as absorbents of natural and functionalized Brazilian bentonite in Pb^{2+} adsorption: Equilibrium, kinetic, pH, and thermodynamic effects

D.J.L. Guerra *, I. Mello, R. Resende, R. Silva

University Federal of Mato Grosso, DRM-UFMT, Mato Grosso 78060 900, Brazil

ARTICLE INFO

Article history:
Received 10 April 2013
Received in revised form
28 October 2013
Accepted 5 November 2013

Keywords:
Adsorption
Bentonite
Lead
Functionalization
Calorimetry

ABSTRACT

The capacities of natural and modified Brazilian bentonite samples as adsorbents to remove lead were investigated under several conditions in batch and column methods. The raw material, natural bentonite, was modified by anchorament of 3-aminopropyltrietoxisilane (APS) and 3,2-aminoethylaminopropyltrimetoxisilane (AEAPS) in the surface of component minerals of bentonite sample. Adsorption behavior of three bentonite types was strongly depending on pH of adsorbate solution, contact time adsorbent/adsorbate, and initial concentration of metal. The maximum adsorption capacities of bentonite types were 20.6843, 27.6524, and 29.5413 mg g^{-1} for natural, bentonite functionalized by APS, and bentonite functionalized by AEAPS, respectively. The results were confirmed by column method and show that the adsorption process of materials accorded with Sips and Langmuir isotherm models. The pseudo-second-order model simulation was also introduced to reveal the principles of the lead removal. The exothermic enthalpic values reflected a favorable energetic process for lead atoms anchored in the material surfaces. The original and modified bentonite samples were characterized by elemental analysis, scanning electron microscopy, and X-ray diffraction powder. The negative Gibbs free energy results supported the spontaneity of three adsorption reactions with Pb^{2+}.

© 2013 The Authors. Published by Elsevier B.V.
Open access under CC BY-NC-ND license.

* Corresponding author. Tel./fax: +55 65 30253915.
E-mail addresses: denis@cpd.ufmt.br, dlguerra@pq.cnpq.br (D.J.L. Guerra).

2212-3717 © 2013 The Authors. Published by Elsevier B.V. Open access under CC BY-NC-ND license.
http://dx.doi.org/10.1016/j.wri.2013.11.001

Nomenclature

N_f	the maximum adsorption capacity of the adsorbent (mmol g^{-1})
C_S	metal concentration at equilibrium (mmol dm^{-3})
N_L	amount of adsorbate adsorbed at the equilibrium—Langmuir (mmol g^{-1})
K_L	Langmuir affinity constant (dm^{-3} $mmol^{-1}$)
K_F	Freundlich constant related to adsorption capacity [mmol g^{-1}(mmol $dm^{-3})_F^{-1/n}$]
n_F	dimensionless exponent of Freundlich equation
N_S	amount of adsorbate adsorbed at the equilibrium—Sips (mmol g^{-1})
K_S	Sips constant related to the affinity constant [(mmol $dm^{-3})_S^{-1/n}$]
A_{RP}	the Redlich–Peterson constant (mmol $dm^{-3})^{-g}$
g	dimensionless exponent of Redlich–Peterson equation
K_{RP}	Redlich–Peterson constants (dm^3 g^{-1})
n_S	dimensionless exponent of Sips equation
N_t	amount of adsorbate adsorbed at time t (mmol g^{-1})
N_E	amount of adsorbate adsorbed at the equilibrium—kinetic (mmol g^{-1})
k_{AV}	Avrami kinetic constant (min^{-1})
t	time of contact (min)
k_f	pseudo-first-order rate constant (min^{-1})
k_s	pseudo-second-order rate constant (g $mmol^{-1}$ min^{-1})
α	the initial adsorption rate (mg g^{-1} h^{-1}) of Elovich equation
β	Elovich constant related to the extent of surface coverage and also to the activation energy involved in chemisorption (g mg^{-1})

1. Introduction

Innumerous solid materials, such as hybrid materials modified by organosilane-based self-assembled monolayers, can be used to take up heavy metals from aqueous medium, due to their excellent capacity to absorb pollutants [1–3]. The batch and column adsorption methods are used for removal of pollutants in aqueous and gaseous medium, and the satisfactory results were obtained with these methods and major intendment of mechanism adsorption process in each investigated material. The equilibrium isotherms, thermodynamic data, obtained with Gibbs free equation, and kinetic parameters, obtained by several models such as, Langmuir, Lagergren first-order and second-order isotherm equations were estimated in adsorption process in single and multicomponents systems [4]. The metal adsorption in the phyllosilicate as bentonite types is a very complex process of their structural properties [4–6]. Several investigations on the metallic species [4], dark compounds [5] and pollutant gases [6] adsorption of bentonite clays have been reported.

Silicates and hybrid silicates like organoclays are widely used as adsorbents due to their textural and physical–chemical characteristics, such as high specific area, pore size diameter, cation exchange capacity, and hydrophilic particles that can be formed on their reactive surfaces. As a petrographical definition, bentonite is a geological material composed of volcanic ashes altered in shallow sea and lagoons areas and generally formed of smectite types, which is a 2:1 mineral, consisting of two tetrahedral sheets (silicon/oxygen) separated by an octahedral sheet (aluminum/oxygen/hydroxyl) [7,8]. The ions with positive charges on the clay surface can be adsorbed onto the bentonite structure owing to the interaction between the negative and positive charges. In addition, bentonite is used in chemical and ceramic industries for fabrication of several ceramic products owing to the rheological properties and such phyllosilicate types are recommended for the fabrication of beds for utilization as desiccators or as dehydrator of several gases. The industrial and environmental applications of bentonite have showed an upsurge of interest in recent years [9].

The chemically modifying surfaces are the research area that has been widely investigated and plays a very important part in applications in many academic and technological fields, such as those

related to ion-exchange reactions and supportscatalytic methods, chemical separation, and sensing/detection, and a perfect catalyst support is obtained, with high pore volume with chemical accessibility and high diffusion rates [7,8]. The insertion process of organic neutral polar molecules into the nanospace void of sheets of layered insoluble nanocompounds leads to well-organized inorganic/organic structural layer materials with high crystallinity and porosity [10–14]. Important advances in the organofunctionalization processes field have been obtained by observing if any property of the lamellar nanocompound charges, by comparing these with those related to the host, as well as to the inserted guest molecules at the end of the process [15–18]. Several investigations on intercalatinga variety of amines, such as secondary, tertiary, cyclic or arylic amines into lamellar compounds have been reported [19,20]. These species are of interest not only in order to further clarify the chemistry of layered metal but also because the process leads to the preparation and characterization of a new intercalated phase of hybrid material [21].

In order to study the capacities of natural and organic bentonite samples to remove lead ions from aqueous medium, batch and column adsorption experiments of Pb^{2+} were conducted on natural and functionalized bentonite samples under various conditions. The chemical modifications were realized with Brazilian bentonite sample, 3-aminopropyltrietoxisilane (APS) and 3,2-aminoethylaminopropyl-trimetoxisilane (AEAPS), such as raw material and intercalating agents, respectively. These new functionalized compounds were characterized through physical and chemical methods. The pseudo-second-order model simulation was also introduced to reveal the principles of the lead removal. The energetic effects caused by Pb^{2+} ions/basic center interactions on bentonite samples at the solid–liquid interface were determined through calorimetric titration procedures. The spontaneity of these metal–organic/inorganic systems reflected in the negative Gibbs free energies and the favorable positive entropic values.

2. Materials and methods

2.1. Reagents and raw material

The raw clay was sampled in the Amazon region, in northern Brazil. The natural bentonite sample, named BBT, with less than 2.0 μm particles, was separated by sedimentation. The cation-exchange capacity (CEC) was measured in order to evaluate the potential use of clay for intercalation, following the ammonium acetate method with concentrations of 2.0 mol dm^{-3} at pH 8.0 and 298 ± 1 K. The result obtained was 98.6 meq./100 g of clay on an air-dried basis. The high perceptual of calcium was observed in clay sample, bentonite sample can be classified as Ca-bentonite. Chemical characterization was also carried out, using analytical techniques that will be described below. The natural silicate sample was activated in a stream of dry nitrogen by heating at 423 ± 1 K for approximately 10 h and used immediately.

Reagent grade solvents were used. The compounds *n*-dodecylamine [$CH_3(CH_2)_{11}NH_2$/ ≥ 99%] (Sigma-Aldrich) and 3-aminopropyltrietoxisilane [$H_2N(CH_2)_3Si(OC_2H_5)_3$/99%] (Sigma-Aldrich) and [3,(2-aminoethyl)aminopropyl]trimetoxisilane [$C_8H_{22}N_2O_3Si$/99%] (Sigma-Aldrich) were used without purification. Other chemicals such as methanol and ethanol were of reagent grade. Stock standard solution 5000.0 mg dm^{-3} of Pb^{2+}, was obtained from primary-standard PbS (Merck) and pH was adjusted by addition of 0.10 mol dm^{-3} of HNO_3 (Aldrich) or NaOH (Aldrich). Doubly distilled deionized water (DDW) was used for the preparation of solutions, wherever required. Solutions of lead were prepared from suitable serial dilution of the stock solution in DDW.

2.2. Chemical modification of BBT

The organobentonite types were synthesized by maintaining the reagent molar ratios as 1:200:50:0.3, respectively, for *n*-dodecylamine, DDW, ethanol, and silylating agents. In the first step, *n*-dodecylamine was mixed with DDW and ethanol and allowed to stir continuously for 45 min. In the second step, a mass of 5.0 g of BBT was added to the mixture and the stirring was continued for

50 min. During this time period the silylating agent 3-aminopropyltrietoxisilane was added drop-wise to form the final hybrid material. Same experimental procedure that was used for functionalization with APS, was utilized for functionalization with [3,(2-aminoethyl)aminopropyl]trimetoxisilane. After addition of silylating agents in the bentonite samples, the resulting mixture was further stirred for 20 h at 291 ± 1 K. At the end of the above process, the material was centrifuged, washed with DDW and air dried at room temperature for 30 h. The final products were named BBT_{APS} and BBT_{AEAPS} and these materials were filtered, washed with toluene and ethanol, and dried under vacuum at 291 ± 1 K for approximately 15 h.

2.3. Batch organofunctionalization study

The effect of pH medium on adsorption for clay samples was evaluated by varying this parameter over the range from 1.0 to 13.0. The pH of the solutions was measured using a pH/Ion, model 450 M, Analyzer, SP, Brazil.

The adsorption experiments were performed by a batchwise method, i.e., by suspending 20.0 mg of BBT, BBT_{APS}, and BBT_{AEAPS} in an aqueous solution (25.0 cm^3) of the Pb^{2+} at concentrations varying from 0.110 to 4.35 mmol dm^{-3}, under orbital stirring for approximately 24 h at 298 ± 1 K [16,17]. The bentonite types were separated by centrifugation and supernatant solutions were carefully transferred to glass flasks to determine the concentrations of lead in aqueous medium. The final concentrations of the lead ions were determined using a Perkin Elmer Flame Atomic Absorption (AA) Spectrometer model Analyst 200 operating with an air–acetylene flame and a lead cathode lamp ($\lambda_{Pb(II)}$=217.00 nm, analytical line=283.30 nm). The Pb^{2+} adsorption capacities (N_f) of the phyllosilicate and intercalating agents were calculated according to Eq. (1), for series of isotherms, revealed that the adsorption process conforms to the equilibrium models. The isotherm equations corresponding to the Langmuir [22], Freundlich [23], and Sips [24] models are presented in Table 1. The kinetic equations corresponding to the Avrami, pseudo-first-order, and pseudo-second-order models [25] are also given in Table 1.

$$N_f = \frac{N_i - N_e}{m} \tag{1}$$

where N_i (mmol) is the initial number of moles of Pb^{2+} added to the surface of clay adsorbent, N_e (mmol) is the amount remaining after the equilibrium of adsorption reactions, and m (g) is the mass of the clay adsorbent. Profiles of the obtained adsorption isotherms were represented by the number of moles per gram bentonite types, N_f (mmol g^{-1}), versus the number of moles at equilibrium per volume of solution of lead, C_S (mmol dm^{-3}). The samples were collected at 0, 10, 20, 30, 40, 50, 60, 70, 80, 90, 100, 110, 120, 130, 140, 150, 160, 170 and 180 min from the conical flask, filtered, and analyzed for lead concentration.

Table 1
Isotherms equilibrium and kinetic adsorption models.

Adsorption models	Nonlinear equations
Isotherms equilibrium models	
Langmuir	$N_f = \frac{N_L K_L C_S}{1+K_L C_S}$
Freundlich	$N_f = K_F {C_S}^{1/n_F}$
Sips	$N_f = \frac{N_S K_S {C_S}^{1/n_S}}{1+K_S {C_S}^{1/n_S}}$
Redlich–Peterson	$N_f = \frac{K_{RP} C_S}{1+A_{RP} C_S^{\beta}}$
Kinetic models	
Avrami	$N_t = N_E[1-\exp[-(k_{AV}t)]^{n_{AV}}]$
Pseudo-first-order	$N_t = -N_E[1-\exp(-k_f t)]$
Pseudo-second-order	$N_t = \frac{N_E^2 k_s t}{1+k_s N_E t}$
Elovich	$N_f = \frac{1}{\beta}\ln(\alpha\beta)+\frac{1}{\beta}\ln t$

2.4. Column-adsorption study

A glass column 15.0 cm long and with 0.50 cm internal diameter, a porous sintered glass disk at the bottom and a Teflon stopcock was packed with 1.00 g of BBT, BBT_{APS}, and BBT_{AEAPS} samples for each adsorption experiment, which occupied 5.0 cm^3 of this column. The column was then filled from the top with 1.50×10^{-4} mol dm^{-3} of the Pb^{2+} at pH 4.0 and 3.0 cm^3 min^{-1} feeding flow rate. The column effluent flow-rate was adjusted to 3.5 cm^3 min^{-1} using the stopcock and the solution depth, or hydraulic head, at the top was kept constant by feeding the column at the same flow rate as the effluent using a peristaltic pump (Model 601, SP, Brazil). The column effluents were collected in 50.0 cm^3 intervals using a fraction collector and Pb^{2+} was determined as above using a Flame Atomic Absorption Spectrometry (Analyst 200, Perkin-Elmer). The column adsorption capacity (N_{ed}) was calculated by the by the following equation [26]:

$$N_{ed} = \frac{(C_0 V_0 - \Sigma C_n V_n)}{m} \tag{2}$$

where N_{ed} (mg g^{-1}) is the amount of Pb^{2+} adsorption per gram of BBT, BBT_{APS}, and BBT_{AEAPS} at saturation, C_0 (mg dm^{-3}) is the original concentration of lead, V_0 (dm^3) is the volume of the effluent solution, C_n (mg dm^{-3}) is the concentration of sample n, V_n (dm^3) is the volume of clay sample n, and m (g) is the amount of clay types.

In order to evaluate BBT, BBT_{APS}, and BBT_{AEAPS} as possible adsorbents for wastewater treatment of Pb^{2+}-containing effluents, breakthrough curves for Pb^{2+} using materials as adsorbents were obtained; the values were determined by analyses of the BP_1 (lower breakpoint) and BP_2 (higher breakpoint), both of which were obtained after passing an effluent volume of 1.50×10^{-4} mol dm^{-3} of Pb^{2+} through the column of adsorbent.

Due to the continuous adsorption, the flow of Pb^{2+} solution creates a wave front as it flows through the bed composed of materials. This wave front is known as the 'mass transfer zone' (MTZ). In order to determine the MTZ, the amount of Pb^{2+} input into the column and the total amount removed were calculated; they correspond to the adsorption capacity until the breakthrough point (q_U), which is BP_2, and the saturation point (q_T), respectively. Eqs. (3) and (4) were obtained through mass balance in the column using its saturation data based on its breakthrough curves, where the area below the curve ($1 - C_t/C_0$) up to the breakthrough point is proportional to q_U, and up to the point of exhaustion of the bed is proportional to q_T [27].

$$q_U = \frac{C_0 V}{1000m} \int_0^{t_b} (1 - C_t|_{Z=L}/C_0) dt \tag{3}$$

$$q_T = \frac{C_0 V}{1000m} \int_0^{t_{tot}} (1 - C_t|_{Z=L}/C_0) dt \tag{4}$$

where q_U (mg g^{-1}) is amount of adsorbent Pb^{2+} per unit of adsorbent mass up to the breakthrough point, C_t (mg dm^{-3}) is Pb^{2+} concentration in a solution in the column outlet, C_0 (mg dm^{-3}) is the initial lead concentration in the liquid state, m (g) is the bentonite mass, t_b (min) is time until breakthrough point, and t_{tot} (min) is time for total removal and limit of concentration in a solution column outlet ($Z=L$).

The mass transfer zone (MTZ) can be calculated based on the q_U/q_T ratio according to Eq. (5). MTZ and has a maximum value which corresponds to the bed height (H_L) [27].

$$\mathrm{MTZ} = H_L \left(1 - \frac{q_U}{q_T}\right) \tag{5}$$

2.5. Thermal effect interactions

The thermal effects from metal cation interacting on BBT, BBT_{APS}, and BBT_{AEAPS} samples were followed by calorimetric titrations using an isothermal calorimeter, Model LKB 2277, from thermometric. In this titration, the lead solution is added to a suspension of about 20 mg of the

solid sample in 2.0 cm^3 of water, under stirring at 298 ± 1 K. A series of increments of 10.0 dm^3 of metal solutions was added to the Pb^{2+}, BBT, BBT_{APS}, and BBT_{AEAPS} to obtain the thermal effect of interactions (ΣQ_t). Two other titrations are needed to complete the full experiment: (i) the thermal effect due to hydration of the bentonite samples (ΣQ_h), which normally gives a null value and (ii) the dilution effect of lead solution in water, without sample in the vessel (ΣQ_d). The resulting thermal (ΣQ_r) effect is given by the following equation [28]:

$$\sum Q_r = \sum Q_t - \sum Q_d - \sum Q_h \tag{6}$$

2.6. Characterization methods

The elemental analysis (%C, %H, and %N) was determined on a Perkin Elmer 2400 Series II microelemental analyzer, and at least two independent determinations were performed for natural and modified clay samples.

X-ray diffraction (XRD) of the clay samples was obtained with a Philips 3020 Goniometer with PW 3710 Controller using Cu Kα radiation at 40 kV and 20 mA and Ni filter.

The original and modified clay samples were analyzed by scanning electron microscopy (SEM) in JEOL microscope, model JEOL JSM 6360LV, using an acceleration voltage of 20 kV and magnification ranging from 200 to 500 fold. EDX analysis was carried out at 80 kV; the bentonite spectrum was collected for 60 s.

The values of Brunauer–Emmett–Teller (BET) surface area, pore diameter and pore volume for each clay sample were obtained from nitrogen adsorption/desorption in a Micromeritics ASAP 2000 BET surface analyzer system. The mesopore size distribution was obtained by applying the Barret–Joyner–Halenda (BJH) method to the adsorption branch of the isotherm. The theoretical BET model for multilayer sorption is given by the following equation [29]:

$$N_f = \frac{BQ^0 C_{Eq}}{(C_S - C_{Eq})[1 + (B-1)(C_{Eq}/C_S)]} \tag{7}$$

where C_S is the saturation concentration, B is the constant indicating the energy of solute–clay surface interaction, C_{Eq} is the equilibrium concentration, and Q^0 is the constant indicating the amount of solute adsorbent forming a complete monolayer.

The density of clay samples was measured using a Micrometrics Accupyec 1330 helium gas pycnometer. The analyses were performed at 298 ± 1 K and 1×10^{-3} psig min^{-1} equilibrium rate.

Sample porosity was measured using a Micrometrics 9400 porosimetry. A 50.000 μm Hg evacuation pressure was utilized for the low-pressure phase, 60 min evacuation time and 30 s equilibrium time, both for the low and high-pressure phase.

3. Results and discussion

3.1. Characterization of clay and organoclay

In these formed 2:1 silicate structures the organic part is distributed inside the interlayer lamellar cavity of interstratified smectite–illite (S–I) and the percentages of carbon, hydrogen, and nitrogen content are listed in Table 2, with the integrity of the organic molecules being present in the dioctahedral 2:1 structure of S–I confirmed from the calculated C/N ratios [30]. Based on the analytical data for BBT and two organic–inorganic materials, the density of these pendant organic molecules immobilized on the tetrahedral silica layer of the phyllosilicate can be calculated. Thus, the precursor H_2N–$(CH_2)_3Si(OC_2H_5)_3$ agent grafted onto bentonite clay gave an amount of 6.942 mmol g^{-1} (BBT_{APS}). In principle, this small pendant molecule density should be expected as a consequence of its large volume, which could cause a degree of hindrance to impede the reaction. The organosilane population density is important for utilization of hybrid material for adsorption process, as this density is directly related to the lattice spacing of the terminal functionality at the monolayer interface. The cation exchange capacities (CEC) of bentonite types were studied in two temperatures, 298 ± 1 K and

Table 2
Surface area (SA_{BET}), real density (RD), porosity, cation exchange capacity (CEC), and percentages of carbon (C), hydrogen (H), and nitrogen (N) for natural and modified bentonite clays and comparison of the properties of natural and modified nontronite with some bentonite samples.

Sample	SA_{BET} ($m^2\ g^{-1}$)	RD ($g\ cm^{-3}$)	Porosity (%)	CEC[a] (mmol/100 g)	CEC[b] (mmol/100 g)	C (%)	H (%)	N (%)	C/N (calculated)	C/N (found)	Reference
BBT	34.1	0.991	29.311	98.6	111.5	0.015	0.0921	–	–	–	Current research
BBT_{APS}	597.3	2.723	68.472	107.7	120.5	4.408	7.891	0.635	6.942	9	Current research
BBT_{AEAPS}	612.3	2.811	72.151	134.9	146.7	1.752	6.789	0.438	4.435	4	Current research
Imp-B	31.5	–	–	88.7	–	–	–	–		–	Xifang et al. [34]
PRYL-B	71.1	–	–	98.4	–	–	–	–	–	–	Xifang et al. [34]
Ca-bentonite	20	–	–	60.68	–	–	–	–	–	–	Shu-li et al. [35]
Na-bentonite	56	–	–	94.30	–	–	–	–	–	–	Shu-li et al. [35]

[a] 98 ± 1 K.
[b] 373 ± 1 K.

373 ± 1 K. The CEC values increased in the high temperature; the CEC values were increased to 8.74%, 11.88%, and 13.08% for BBT_{APS}, BBT_{AEAPS}, and BBT, respectively, in 4 h, at 373 ± 1 K. These variations can be an indication that in adsorption process, these materials may present propensity to physisorption (Table 2).

X-ray diffraction patterns of the BBT, BBT_{APS}, and BBT_{AEAPS} samples are given in Fig. 1a and b. With interstrafied smectite–illite (S–I) as principal clay minerals and quartz (Q) and feldspar (F) as impurities or accessory clay minerals, the raw bentonite clay sample is constituted by the conjunct of these minerals [31]. The bentonite components were concentrated in the fine size fraction (< 2.0 mesh); therefore, an important decrease of quartz and feldspar components was observed after organofunctionalization process, principally in the sample organofunctionalized by AEAPS. In the interstrafied fraction of BBT, the smectite clay was the predominant mineral and illite was the mineral with minor perceptual (Fig. 1b). The Bragg equation was used for determination of d_{001} values and used to calculate the remaining reflections [32]. The 001 peak of the smectite–illite component of the BBT_{APS} and BBT_{AEAPS} samples was narrower and higher than that of the raw bentonite sample, indicating better crystallinity of the organoclays than the BBT; the values of d_{001} were increased with functionalization process and the d_{001} values of BBT_{APS} and BBT_{AEAPS} were 11.20 and 17.01 nm, respectively. The results suggest that the physical–chemical properties were optimized with functionalization process. The insoluble impurities such as quartz and feldspar become more intense by the intercalation process. The intensities of (100), (110), (200), and (210) smectite reflections were increased and presence of material amorphized was not observed with the organofunctionalization process [31,32].

Typical SEM micrographs of powder BBT, BBT_{APS}, and BBT_{AEAPS} are presented in Fig. 2a, b, and c, respectively. The micrographs reveal the heterogeneous nature of surface morphology of the clay sample which also shows that smectite–illite crystals possess a foliated crystal like morphology. In the BBT micrograph was also observed crystals of small size belonging to the hexagonal crystalline system; these crystals can be attributed to the accessory mineral quartz, this is relatively common in the Amazon soil, and the formation of mineral is propitiated by lixiviation of Amazon soil. The crystals of three materials present fissures, which can be the indication of the presence of a macroporous structure. These should contribute a little bit to the diffusion of the organic chain to the silicate adsorbent surfaces, favoring defunctionalization process and posteriorly the removal of divalent metals. Chemical analyses for BBT sample presented the presence of silicon, aluminum, magnesium,

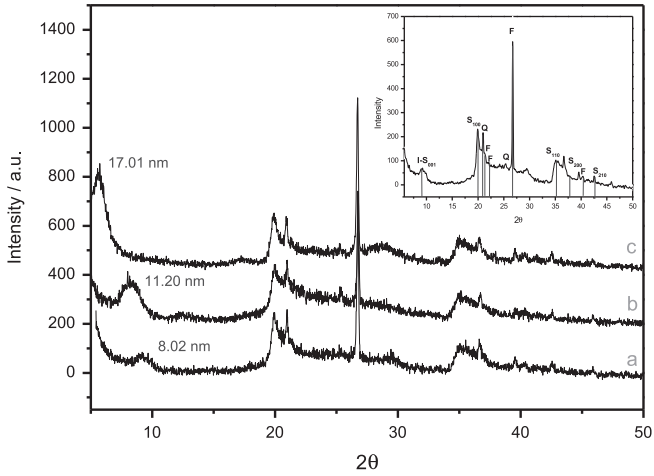

Fig. 1. X-diffraction patterns of the bentonite types: BBT (a); BBT_{APS} (b); and BBT_{AEAPS} (c) and original bentonite sample with component minerals.

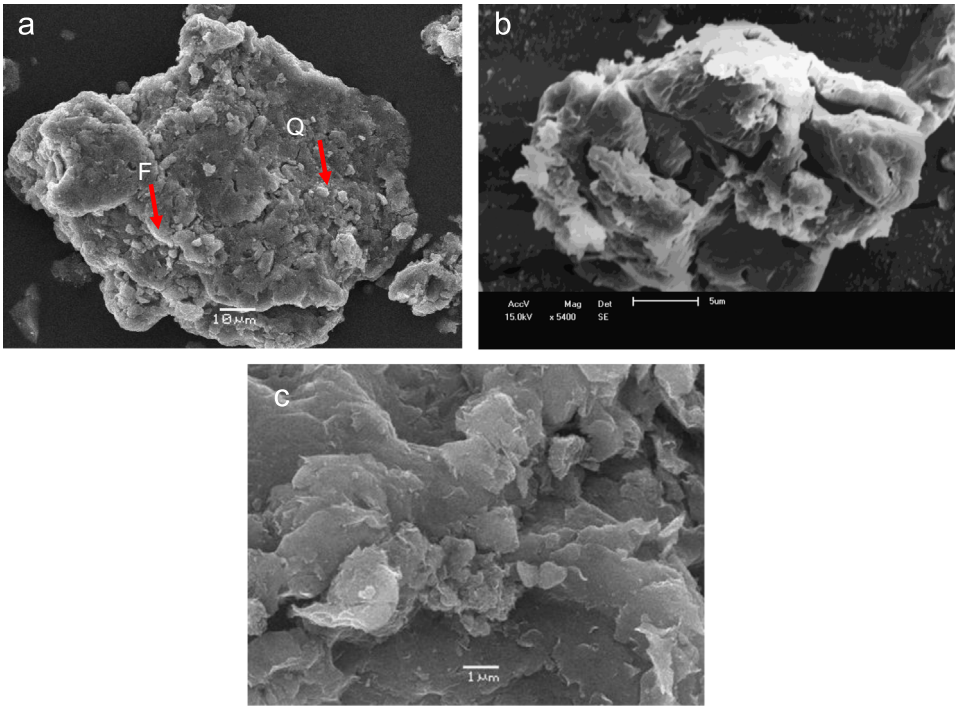

Fig. 2. SEM micrographs of the natural and modified bentonite types: BBT (a), BBT_{APS} (b) and BBT_{AEAPS} (c).

and iron that was observed which can be attributed to principal component (S–I) and accessory minerals (Q and F); the small perceptual of carbon present could be attributed to remnants of organic material from humic acids which naturally adhered to mineral surface [33].

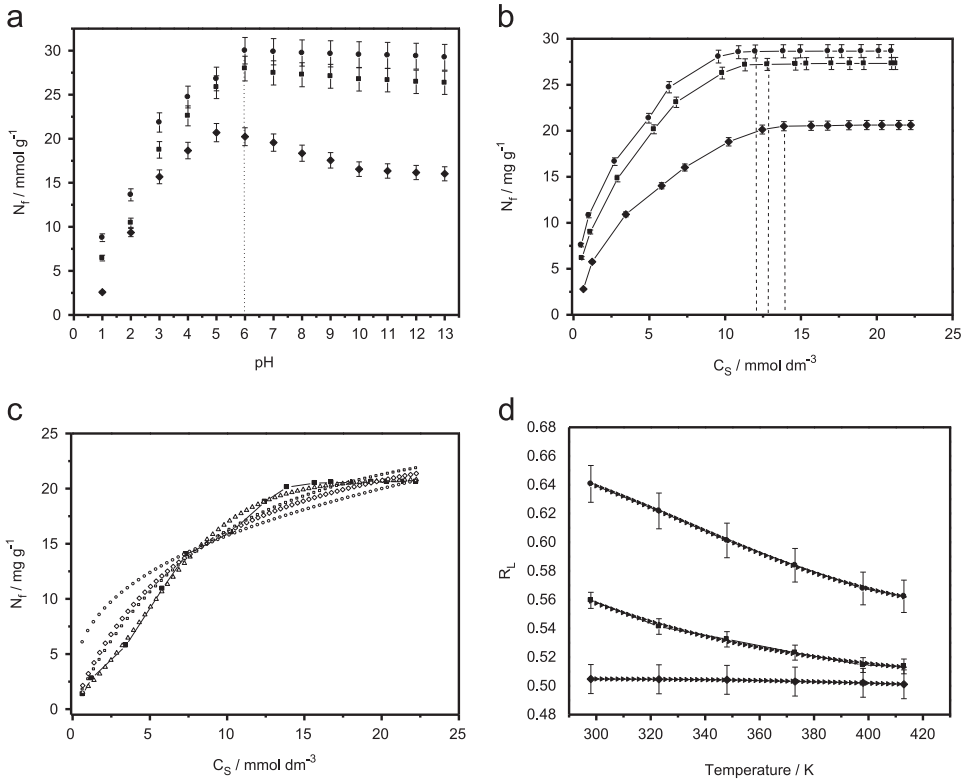

Fig. 3. Effect of pH on Pb^{2+} adsorption (a) effect of concentration of Pb^{2+} adsorption onto bentonite types (b): BBT ◆; BBT_{APS} ■; and BBT_{AEAPS} ●, Isotherms calculated with non-linear method: Sips Δ; Langmuir □; Freundlich ○; and Redlich–Peterson ◊ (c) and separation factor of Pb^{2+} ions adsorbed on six different temperatures (d).

The textural analyses have been important for investigation of the reactive centers in the surface of functionalized materials. The surface area of a porous organoclay is one of the most useful microstructural parameters for defining properties. The BET surface areas of the natural and modified bentonite samples demonstrated that chemical modification caused the formation of micropores in the solid particles, resulting in a higher surface area, revealing 612.3 $m^2\ g^{-1}$ for BBT_{AEAPS} and relative to the natural BBT sample with 34.1 $m^2\ g^{-1}$. The values of micropore area change in the same direction, varying from 7.2 $m^2\ g^{-1}$ for the BBT to 12.3 $m^2\ g^{-1}$ for the BBT_{AEAPS}. The textural properties of natural and modified bentonite samples which are reported in Table 2, depend on particle size shape, and distribution of cracks and pores in the material, the surface area and CEC of bentonite samples used and obtained in this study, were compared with other bentonite samples studied by Xifang et al. [34] and Shu-li et al. [35]. The BBT_{AEAPS} has a significantly higher surface area than the BBT and has pores < 2 nm in diameter (micropore) in addition to some mesopores (> 4 nm diameter). The natural bentonite has small N_2 BET surface areas and only mesopores because N_2, as opposed to H_2O, OH^-, and H_3O^+, is unable to penetrate into the octahedral position in structure of interstratified smectite–illite may have in the center a vacancy.

3.2. *Adsorption: effect of pH and variation of concentration of Pb^{2+}*

Adsorption process has been shown to be the best alternative for all pollutant organics and inorganics for the removal from aqueous medium, clays and organoclays being the most efficient adsorbent for this process due to their easy synthesis, versatility, and abundant natural occurrence.

The adsorption process in diluted solution, at constant temperature and pressure can be described by the following generic reaction:

$$A_{SOL} + B_{ADS} \leftrightarrow A_{ADS} + B_{SOL} \quad (8)$$

where A_{SOL} is the solute in solution, B_{ADS} is the adsorbed solvent, A_{ADS} is the adsorbed solute, and B_{SOL} is the solvent in solution. The adsorbent capacity of material for removal contaminants can be investigated through of batch method. The Pb^{2+} ions were examined within a range of pH 1.0–13.0. Fig. 3a shows the influence of pH in adsorption process of Pb^{2+} onto surfaces of BBT, BBT_{APS}, and BBT_{AEAPS}. The data reveals maximum values of N_f^{max} around pH 5.0 for BBT and 6.0 for BBT_{APS} and BBT_{AEAPS}. As can be seen from Fig. 3a, the adsorption of Pb^{2+} on BBT mainly occurs at $5.0 < pH < 9.0$. The adsorption of Pb^{2+} increases quickly at $pH < 8.0$ for BBT_{APS} and BBT_{AEAPS}. Results emphasize that with increase in pH of solution, the N_f^{max} adsorbed increases for three systems. Therefore the efficiency of Pb^{2+} on surface of materials can be controlled by the initial pH of the solid–liquid reactions. The reason for low adsorption capacity in high pH is the competition between the excess of OH^- species in the solutions [36]. Also, higher acid concentrations suppress hydrolysis of the Pb^{2+} ions; the metal immobilization in the surface of materials was favored by the acidification of medium. In addition, the adsorption of Pb^{2+} ions on surface material types is principally dominated by ion-exchange or outer-sphere complexation at low pH values, and by inner-sphere complexation at high pH [37]. Consequently the number of moles of Pb^{2+} removal may decrease at low pH.

From the adsorption isotherm for Pb^{2+} ions, represented by a C_s versus N_f plot, the calculated curves were obtained with non-linear method, as shown in Fig. 3b, whose data were adjusted to the Langmuir, Freundlich, Sips, and Redlich–Peterson models (Fig. 3c), as before. The Sips adsorption model can be used to explain the significant capacity of the BBT to quantify divalent metal interaction by complexation reactions. The four theoretical models present a significant advantage in comparing the experimental data; it allows quantifying the capacity of retaining cations within the structure of the bentonite types and to evaluate the constant related to the bonding energy.

The equation to the Sips equation can also be obtained by assuming that the reactive surfaces of material adsorbent are homogeneous, but that the adsorption is a cooperative and a complex process due adsorbate–adsorbent interaction. One of the essential characteristics of Langmuir model and derivative models, such as Sips model could be expressed by a dimensionless constant called equilibrium parameter or dimensionless separation factor, R_L which can be calculated by the following equation [38]:

$$R_L = \frac{1}{(1 + K_L C_0)} \quad (9)$$

where C_0 is the highest initial solute concentration (mmol dm^{-3}). The parameters of Langmuir equation may be utilized to represent the affinity in the adsorption process between adsorbent and adsorbate surfaces using the dimensionless separation factor and the criteria for separation factor and characteristics of Langmuir isotherms, are $R_L > 1$ is unfavorable, $R_L = 1$ is linear, $0 < R_L < 1$ is favorable, and $R_L = 0$ is irreversible [38]. As seen in Fig. 3d, the values of R_L for adsorption of Pb^{2+} on bentonite surfaces at six different temperatures ($T_n = 298$, 323, 348, 373, 393, and 413 ± 1 K) were between 0 and 1, which indicates favorable adsorption of lead on surface of materials that were utilized in this study as adsorbents.

3.3. Kinetic of Pb^{2+} adsorption and effect of adsorption temperature

The adsorption experimental data for Pb^{2+} uptake versus contact time for a fixed adsorbent amounts are presented in Fig. 4a, giving identical, abrupt increase in adsorption at low times before reaching the plateaus. According to these data, equilibrium is achieved at around 100 and 120 min for systems Pb^{2+}/BBT_{APS}, Pb^{2+}/BBT_{AEAPS}, and Pb^{2+}/BBT. However, to be sure of the best adsorption conditions at higher concentrations levels, to obtain equilibrium at the solid–liquid interface, all the experiments were carried out with 180 min of contact time. This short time period required to attain equilibrium suggests an excellent affinity of the lead for these materials, principally in the adsorption process with modified bentonite from aqueous solution. The most accurate prediction of the

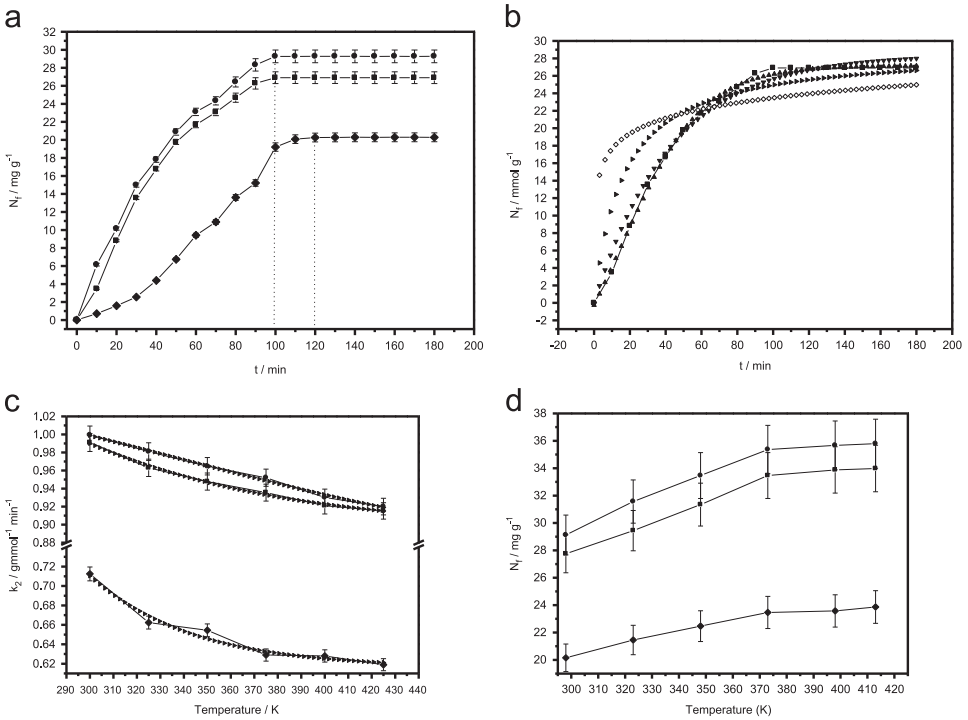

Fig. 4. Kinetics of adsorption: experimental curves (a), BBT ◆; BBT_{APS} ■; and BBT_{AEAPS} ●; theoretical curves: firth-order ▼; pseudo-second-order ▲; Avrami ►; and Elovich ◊ (b), activation energy calculated by non-linear of Arrhenius equation ► (c) and effect of temperature in adsorption process (d).

experimental data was achieved by the pseudo-second order model, indicating that the chemisorption rate seems to be the controlling step in the procedure, i.e., when the rate of reaction of an adsorption reaction is controlled by chemical exchange, then a pseudo-second order Lagergren model can be better adjusted to the experimental kinetic data, this model is also based on the adsorption capacity of the solid phase [39], as expressed in Table 3. Carrying out a set of experiments at constant temperature (273 ± 1 K) and monitoring the amount adsorbed with time, the kinetics of the adsorption process should be known. The rate of metal uptake during the entire period of adsorption was found to be independent of metal initial concentration used. The correlation coefficient of the pseudo-second-order rate equation (R^2) for the non-linear regression was approximately 0.99, which suggests that the kinetic adsorption can be described by the pseudo-second-order rate equation with satisfactory approximation of experimental kinetic curve.

Based on the pseudo second-order model, the initial adsorption rate and half-adsorption time are estimated by the following equations [40]:

$$h = k_2 N_{fEQ}^2 \tag{10}$$

$$t_{1/2} = \frac{1}{k_2 N_{fEQ}} \tag{11}$$

The half-adsorption time $t_{1/2}$ is another parameter defined as the time required for the adsorption to take up half as much Pb^{2+} ions as its equilibrium values for three systems. Thus, the initial adsorption rate and half-adsorption time are usually a measure of adsorption rate.

For determination of activation energy E_a (kJ mol^{-1}) for Pb^{2+} adsorption reaction, the pseudo-second-order rate constant k_S was expressed as a function six different temperatures T_n (298, 323,

Table 3
Isotherms equilibrium and kinetic adsorption parameters (at 298 ± 1 K).

Adsorption models	Parameter values		
	BBT	BBT_{APS}	BBT_{AEAPS}
Isotherms equilibrium models			
Langmuir			
N_L (mmol g^{-1})	10.0142	13.2813	14.6530
K_L (dm^3 $mmol^{-1}$)	0.4222	0.5671	0.6156
R^2 adjusted	0.9856	0.9876	0.9987
F_{error}	0.2347	0.2156	0.1256
Freundlich			
K_F [mmol g^{-1} (mmol $dm^{-3})_F^{-1/n}$]	0.8723	0.9127	1.0081
n_F	0.5178	0.7123	0.9167
R^2 adjusted	0.9751	0.8925	0.9461
F_{error}	0.6143	0.7568	0.7001
Sips			
N_S (mmol g^{-1})	9.9978	13.1915	14.2234
K_S (mmol $dm^{-3})_S^{-1/n}$	0.7814	0.9124	0.9367
n_S	0.5612	0.7127	0.7618
R^2 adjusted	0.9998	0.9999	0.9997
F_{error}	0.0117	0.0012	0.0026
Kinetic models			
Avrami			
N_S (mmol g^{-1})	10.6781	13.9871	14.8854
k_{AV} (min^{-1})	0.6123	0.7125	0.9754
n_{AV}	0.3456	0.6731	0.7312
R^2 adjusted	0.9637	0.9721	0.9872
F_{error}	0.4512	0.3781	0.2879
Pseudo-first-order			
N_S (mmol g^{-1})	9.9867	13.2145	14.6891
k_f (min^{-1})	0.7221	0.8153	0.9887
R^2 adjusted	0.9856	0.9845	0.9967
F_{error}	0.6775	0.7176	0.7566
Pseudo-second-order			
N_S (mmol g^{-1})	9.9712	13.2134	14.1923
k_s (g $mmol^{-1}$ min^{-1})	0.7761	0.8145	0.9198
h (mmol g^{-1} min^{-1})	77.1636	142.1893	185.2673
$t_{1/2}$	0.1292	0.0929	0.0766
R^2 adjusted	0.9999	0.9998	0.9997
F_{error}	0.0010	0.0013	0.0024

348, 373, 393, and 413 ± 1 K) by Arrhenius type relationship as follows [41]:

$$k_S = k_0 \exp\left(\frac{E_a}{RT}\right) \tag{12}$$

where k_0 is the temperature independent factor (g mol^{-1} min^{-1}). From this equation and non-linear method, the rate constant values of adsorption, k_0 and the activation energy values are presented in Table 4. These values show that adsorption processes of Pb^{2+} by adsorbent surfaces of materials used in this work are exothermic. These results may be explained by the fact that the adsorption phenomena in three systems are exothermic and spontaneous processes, confirming the conclusion obtained by calorimetric method; the values of determination coefficient (R^2) for both calculated curves were approximately 0.999. The pseudo-second-order kinetic constant decreased with increasing temperature (Fig. 4b). The pseudo-second order kinetic model constitutes a mass action rate model where the surface diffusivity is inversely proportional to the square of concentration of vacant sites in reactive surface of solid.

The effects of six different adsorption temperatures (T_n=298, 323, 348, 373, 393, and 413 ± 1 K) on removal efficiency for Pb^{2+}/BBT_{APS}, Pb^{2+}/BBT_{AEAPS}, and Pb^{2+}/BBT are shown in Fig. 4d; it revealed that removal efficiency for three systems studied increases with the rise of adsorption temperatures. The lead removal efficiency was increased by 15.40%, 13.37%, and 11.22% for BBT_{APS}, BBT_{AEAPS}, and BBT, respectively, in 4 h, at 413 ± 1 K. It is known that the adsorption of metals on the surfaces of the materials can be normally classified as two routes: physisorption and chemisorption. Adsorption of metal through physisorption is considered to be reversible and favorable at low temperature. Obviously enhancement of lead removal by the rise in temperature suggested that the removal of lead on these bentonite types was mainly by chemisorption.

3.4. Thermodynamic effects of Pb^{2+} adsorption

For a series of calorimetric titrations, the number of increments and the volumes of Pb^{2+} ions needed to saturate the mass of the bentonite types [12] are listed in Table 4. The adsorption process was evaluated from the results obtained, by considering the adsorption isotherms and the molar fraction of the Pb^{2+} ions in solution. The experimental data were better adjusted to a Sips model ($R^2 \sim 0.99$), in which it assumed that monolayer of Pb^{2+} ions is formed on the BBT, BBT_{APS}, and BBT_{AEAPS} surfaces. The maximum adsorption capacities for Pb^{2+} onto materials used in this work are listed in Table 4, in which values are highest for BBT_{APS} and BBT_{AEAPS}. The values obtained by Sips model were used together with calorimetric data for thermal effect analyses of the adsorption process of lead. The molar fraction of Pb^{2+} ions in the supernatant in equilibrium for each point of the calorimetric titration (X) was calculated by considering the number of moles of the solute (N_s) and the number of moles of water (N_{wat}) as follows [30]:

$$X = \frac{N_S}{(N_S + N_{wat})} \tag{13}$$

The calculated X values and the data obtained from calorimetry were adjusted to the modified Langmuir isotherm model [42] and are given by Eq. (14). The thermodynamic values obtained were adjusted by the Levenberg–Marquardt criteria and interactions calculated by the Simplex methods. The calorimetric results are presented in Fig. 5a and are listed in Table 4.

$$\frac{\sum X}{\sum \Delta_r h} = \frac{1}{(K_L - 1)\Delta_{int} h} + \frac{\sum X}{\Delta_{int} h} \tag{14}$$

where $\Sigma\Delta_r h$ is the thermal effect of interaction of Pb^{2+} by BBT, BBT_{APS}, and BBT_{AEAPS} surfaces, $\Delta_{int} h$ is the thermal effect of formation of the monolayer formed by metal ions on the mineral surfaces, and K_L is a proportionality constant that also includes the equilibrium constant.

The thermal effects data obtained from the calorimetric titrations were used in a $\Sigma\Delta_r h$ versus ΣX plot and the linearized form is given by a $\Sigma X/\Sigma\Delta_r h$ versus ΣX plot [30,42]. From the enthalpy of formation of monolayer $\Delta_{int} h$ and the number of moles of Pb^{2+}, N_s, adsorbed, on the clay structure, the enthalpies of interaction can be calculated as follows:

$$\Delta_{int} H = \frac{\Delta_{int} h}{N_S} \tag{15}$$

Variation in free energy ($\Delta_{int} G$), enthalpy ($\Delta_{int} H$), and entropy ($\Delta_{int} S$) are important thermodynamic parameters that were determined using the following equations (Eqs. (16) and (17)), taking these values into account [43]:

$$\Delta_{int} G = -RT \ln K_L \tag{16}$$

where K_L (dm^{-3} $mmol^{-1}$) is the equilibrium constant obtained from the Langmuir isotherm equation, T (K) is the absolute temperature, and R (8.314×10^{-3} kJ K^{-1} mol^{-1}) is the universal gas constant. Eq. (17) relates the energy of adsorption systems [43].

$$\Delta_{int} G = \Delta_{int} H - T\Delta_{int} S \tag{17}$$

The thermodynamic cycle for this series of adsorptions involving suspension (susp) of BBT, BBT_{APS}, and BBT_{AEAPS} (BBT_x) in aqueous solution (aq) with Pb^{2+} ions (M^{n+}), $n \rightarrow 2$ can be represented by the

Table 4
Equilibrium, parameters of Adams–Bohart and Arrhenius equations, and thermodynamic data for Pb^2 interaction onto original and modified bentonite samples.

Samples	N_F^{max}[a] (mg g^{-1})	N_F^{max}[b] (mg g^{-1})	q_T (mg g^{-1})	q_U (mg g^{-1})	MTZ	k_{AB} (dm^3 mmol min^{-1})	N_0 (mmol dm^3)	E_a (kJ mol^{-1})	k_0	$-\Delta_{mon}h$ (J g^{-1})	$-\Delta_{mon}H$ (kJ mol^{-1})	$-\Delta_{mon}G$ (kJ mol^{-1})	$\Delta_{mon}S$ (JK^{-1} mol^{-1})
BBT	20.0580	20.6843	7.9132	6.0245	3.0584	0.022	5325	25.51	0.689	69.1 ± 0.1	6.9 ± 0.1	21.2 ± 0.2	49.1 ± 0.1
BBT_{APS}	27.7321	27.6524	12.3561	10.5136	1.8628	0.011	12,418	30.16	0.877	85.0 ± 0.3	6.4 ± 0.1	24.1 ± 0.3	58.2 ± 0.1
BBT_{AEAPS}	29.9414	29.5413	13.0534	11.0254	1.0103	0.010	12,632	31.76	0.901	90.8 ± 0.1	6.2 ± 0.1	24.8 ± 0.1	59.1 ± 0.5

[a] Batch experiment.
[b] Column experiment (material 1.0 g dm^{-3}, pH 4.0, time 3.5 h, and temperature of 298 ± 1 K).

following calorimetric reactions. Reactions (18)–(20) represent calorimetric titration experiment carried out in triplicate for each determination [30,42]

$$BBT_{x(susp)} + M^{n+}_{(aq)} \rightarrow BBT_x.M^{n+}_{(susp)} \quad \sum Q_t \tag{18}$$

$$BBT_{x(susp)} + nH_2O \rightarrow BBT_x.nH_2O_{(aq)} \quad \sum Q_h \tag{19}$$

$$M^{n+}_{(aq)} + nH_2O \rightarrow M^{n+}.nH_2O_{(aq)} \quad \sum Q_d \tag{20}$$

The thermal effects of reactions (13)–(15) for each experimental point of the calorimetric titration were considered in the calculation of the resulting thermal effect (ΣQ_r) of these interactions, as represented by the following reaction:

$$BBT_x.nH_2O_{(aq)} + M^{n+}.nH_2O_{(aq)} \rightarrow BBT_x.M^{n+}_{(susp)} + 2nH_2O \quad \sum Q_r \tag{21}$$

The thermodynamic data are presented in Table 4. From the thermodynamic point of view, the obtained exothermic and positive entropic values establish the set of favorable results for the thermodynamic of Pb^{2+}–BBT_x interactions. Thus, the spontaneities of such reactions are expressed by the negative Gibbs free energy with a considerable contribution of the positive entropy [30,42]. These values suggest that, during interactions Pb^{2+} ions and reactive sites on the clay surfaces, the desolvation disturbs the structure of clay and of the reaction medium to promote the disorganization of the system and, consequently, leads to an increase in entropy [30,42]. Relationship between

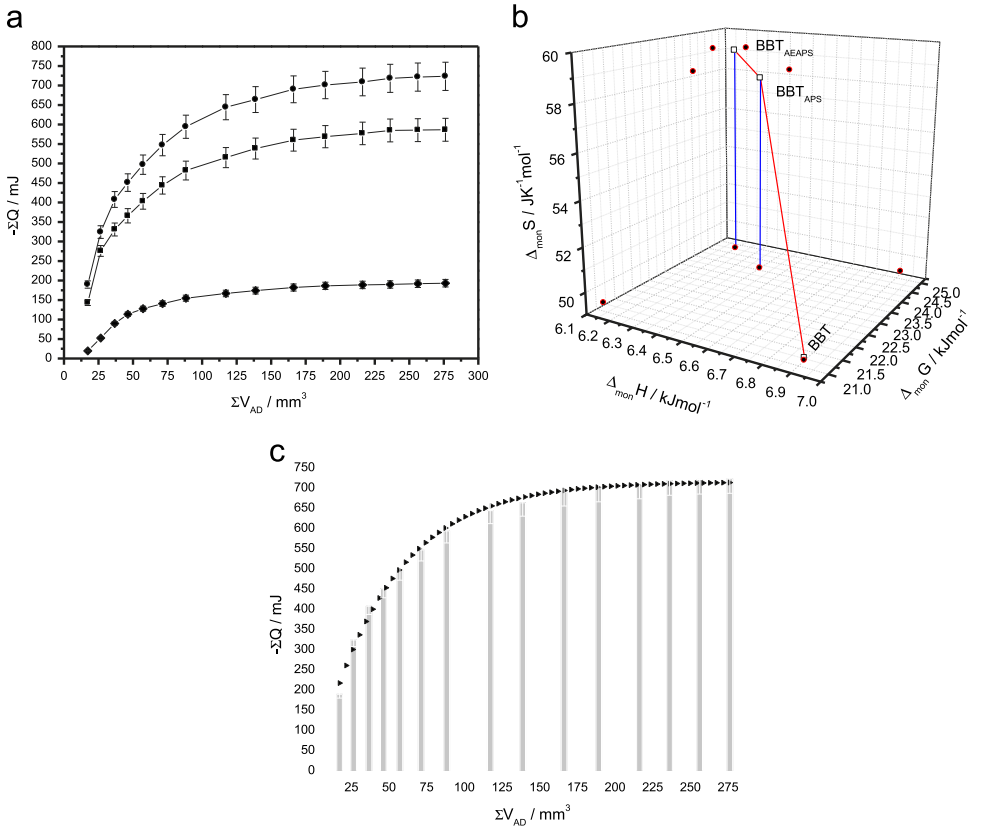

Fig. 5. Isotherms of thermal effects for Pb^{2+} adsorption for bentonite types: BBT ◆; BBT_{APS} ■; and BBT_{AEAPS} ● (a), relationship between thermodynamics adsorption values for three systems (b), and an example of isotherm calculated with non-linear method (BBT_{AEAPS}/Pb^{2+}) (c).

thermodynamics adsorption values for three systems is presented in Fig. 5b and an example of isotherm calculated with non-linear method for system BBT_{AEAPS}/Pb^{2+} is presented in Fig. 5c. In conclusion, all thermodynamic values are favorable, with exothermic enthalpy, negative free Gibbs energy and positive entropy, data corroborate with Pb^{2+}–BBT_x interactions at the solid–liquid interface.

3.5. Column Pb^{2+} adsorption

The removal capacities of continuous packed bed are described through the concept of the breakthrough curves. The breakthrough curves are usually expressed in terms of concentration defined as the ratio of the effluent pollutant concentration to inlet pollutant concentration (C_t/C_0) as a function of time for a given bed height. In order to evaluate BBT, BBT_{APS}, and BBT_{AEAPS} as absorbents for wastewater treatment of lead containing effluents, breakthrough curves of this divalent metal using bentonite types as absorbents were obtained, as illustrated in Fig. 6a. The layer structure of the modified bentonite, BBT_{AEAPS}, is less stable than the natural bentonite as signalized by the formation and fragmentation of clusters of particles during the adsorption tests in column-flow conditions. Smaller breakthrough points (BP_1) were determined when the lead ion effluents from the column attained concentrations of $> 0.010\ mg\ dm^{-3}$, with the curve showing an S-type model [44].

Adams–Bohart equation with fundament on the reactions on surfaces of adsorbent materials and non-spontaneity the equilibrium of reactions in the adsorbent surface; accordingly, the rate of the adsorption is considered proportional to the fraction of adsorption capacity still that remains on the adsorbent. The Adams–Bohart model is utilized for the analysis of the initial part of the breakthrough experimental curves and the nonlinear form of model is given by the following equation [26]:

$$\frac{C_t}{C_0} = \exp\left[k_{AB}C_0 t - k_{AB}N_0\frac{Z}{U_0}\right] \tag{22}$$

where C_0 ($mg\ dm^{-3}$) and C_t ($mg\ dm^{-3}$) are the inlet and effluent metal concentrations, respectively. Z (cm) is the height of the column, U_0 ($cm\ min^{-1}$) is the superficial velocity, N_0 ($mg\ dm^{-3}$) is saturation concentration adopted for this model, and k_{AB} ($dm^3\ mg^{-1}\ min^{-1}$) is the mass-transfer coefficient. The range t should be considered from the beginning to the final part of breakthrough. From the Adams–Bohart model, values describing the characteristic operational parameters of the dynamic system can be determined from a plot of C_t/C_0 against t at a given bed height and flow rate

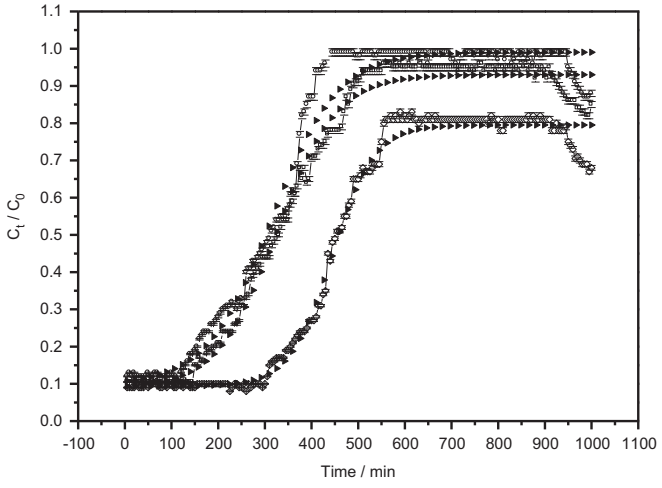

Fig. 6. Effect of variation influent concentration on the breakthrough curves for bentonite types, BBT ◇, BBT_{APS} □, and BBT_{AEAPS} ○ and curves calculated with non-linear method by Adams–Bohart equation ►.

and complete time-dependent analytical solutions to differential equation based models of the proposed rate mechanisms are not available (Fig. 6b).

The BP_1 value is related to the capacity of the adsorbents to retain the Pb^{2+} ions from aqueous solutions. The large breakpoints (BP_2) were related to the complete saturation of the materials with the lead ions. Using an adsorption column packed with adsorbent reactive sites in which an inert carrier flows at a steady rate (a dynamic system), the BP_1 value clearly indicated that the bentonite types would be efficient adsorbents assisting in the decontamination of effluents of divalent metal lead [45]. A single volume of the adsorbent is capable of at least 2.25 mmol g^{-1} of lead as observed for BBT_{AEAPS}. The values for Pb^{2+} adsorption in a dynamic system were similar to values obtained in batch experiments (Table 4). Using a dynamic adsorption system, the maximum saturation of the materials by Pb^{2+} is very close to the values obtained in the batch-adsorption experiments for three systems in this study.

4. Concluding remarks

The efficiency of adsorption process with the raw and hybrid materials used in this study depends not only on the chemical and physical properties of the adsorbate, but also on the composition of medium. pH, concentration of medium and time of contact metal–surface are two or more selected parameters investigated as the characteristics of aqueous medium affecting material capacities. The results obtained can be summarized as follows:

(i) The removal of Pb^{2+} by surface materials as BBT, BBT_{APS}, and BBT_{AEAPS} is a complex phenomenon, principally in the heterogeneous surfaces, such as BBT_{APS} and BBT_{AEAPS}. The update of lead from aqueous medium strongly depends on pH solution, the most appropriate condition was pH range 6.0–8.0 at 298 $\pm$ 1 K. The maximum adsorption capacity was observed at pH 5.0 for system Pb^{2+}/BBT and 6.0 for systems Pb^{2+}/BBT_{APS} and Pb^{2+}/BBT_{AEAPS}.

(ii) The Langmuir, Freundlich, Sips, and Redlich–Peterson theoretical isotherms were utilized to interpret the experimental adsorption data; the Sips model was the model that best represented the equilibrium data. The pseudo second-order model provided the best correlation of the experimental kinetic data. Measured values of model constants indicated significant differences in the curve shapes and adsorption capacities regarding natural and organobentonite in reaction with lead ions. The considerable period required to establish adsorption equilibrium may indicate that the adsorption process can be controlled by physical adsorption.

(iii) The adsorption results were confirmed through stable complexes formed between cations and reactive groups disposed on the natural and organobentonite surfaces, whose behavior was checked by the thermodynamic values obtained by calorimetric investigations at the solid–liquid interface to give favorable sets of data; thermodynamic values calculation showed that the Pb^{2+} adsorption process by materials has exothermic and spontaneous nature, such as exothermic enthalpy, negative Gibbs free energy, and positive entropic values. The adsorption process of Pb^{2+} on natural bentonite and modified bentonite samples were controlled by chemical and physical mechanisms.

(iv) Dynamic flow tests showed that the adsorption of lead onto material surfaces on flow rate of adsorbate, inlet feed Pb^{2+} concentration and permanence time solid–liquid and the experimental data is well fitted by Admas–Bohart equation. Comparing the batchwise method and column experiments, batchwise method effectively exploited the adsorbent divalent metallic cation binding capacity rather than fix bed column. For industrial and environmental application of adsorption with potentiated hybrid surfaces, organofunctionalization with alkylamines is necessary for full separation of solid–liquid.

(v) Actually a wide variety of adsorbent materials is utilized for the adsorption of a broad range of pollutants; the ideal adsorbent mandatorily should have interesting characteristics for industrial and environmental applications, in this context, is possible to conclude that the clay and organoclays employed are more economical than commercially available adsorbentsthat were applied industrially for batch and dynamic flow method. Temperature, pH effluence, effect of concentration variation, and contact time will be important parameters affecting the adsorption

capacity in the real application in the removal process. The majority of water industries contaminated with Pb^{2+} from inopportune technical operations contain more than one toxic heavy metal; consequently, adsorption in batch and dynamic flow involves competitive ion exchange, in which several toxic heavy metals compete for a limited number of binding sites.

Conflict of Interest

The authors declare no conflict of interest.

Acknowledgments

The authors are grateful to MCT, CNPq, and CAPES for financial support and fellowships.

References

[1] J.P. Rawat, A.A. Ansari, R.P. Singh, Sorption equilibria of lead(II) on some Indian soils—the natural ion exchangers, Colloids Surf. 50 (1990) 207–214.
[2] U.M. Saha, K. Iwasaki, K. Sakurai, Desorption behavior of Cd, Zn, and Pb sorbed on hydroaluminum and hydroaluminosilicate–montmorillonite complexe, Clays Clay Miner. 51 (2003) 481–492.
[3] D.L. Guerra, E.M. Silva, W. Lara, A.C. Batista, Removal of Hg(II) from an aqueous medium by adsorption onto natural and alkil-amine modified Brazilian bentonite, Clays Clay Miner. 59 (2011) 568–580.
[4] M. Carabasa, A. Ibarz, S. Garza, G.V. Barbosa-Cánovas, Removal of dark compounds from clarified fruit juices by adsorption process, J. Food Eng. 37 (1998) 25–41.
[5] S.S. Tahir, N. Rauf, Thermodinamic studies of Ni(II) adsorption onto bentonite from aqueous solution, J. Chem. Thermodyn. 35 (2003) 2003–2009.
[6] J.L. Venaruzzo, C. Volzone, M.L. Rueda, J. Ortiga, Modified bentonitic clay minerals as adsorbent of CO, CO_2 and SO_2 gases, Microporous Mesoporous Mater. 56 (2002) 73–80.
[7] A. Meunier, Clays, Springer, Berlin Heidelberg, New York472.
[8] G. Bulut, M. Chimeddorj, F. Esenli, M.S. Çelik, Production of desiccants from Turkish bentonite, Appl. Clay Sci. 40 (2009) 141–147.
[9] A. Bojumueller, G. Nennemann, G. Lagaly, Enhanced pesticide adsorption by thermally modified bentonites, Appl. Clay Sci. 18 (2001) 277–284.
[10] D.L. Guerra, V.P. Lemos, C. Airoldi, R.S. Angélica, Influence of the acid activation of pillared smectites from Amazon (Brazil) in adsorption process with butylamine, Polyhedron 25 (2006) 2880–2890.
[11] D.L. Guerra, R.R. Viana, C. Airoldi, Adsorption of mercury cation on chemical modified clay, Mater. Res. Bull. 44 (2009) 485–491.
[12] A.M. Lazarin, C. Airoldi, Thermodynamic of the nickel and cobalt removal from aqueous solution by layered crystalline organofunctionalized barium phosphate, J. Chem. Thermodyn. 41 (2009) 21–25.
[13] F. Wypych, W.H. Schreiner, N. Mattoso, D.A. Mosca, R. Marangoni, C.A.S. Bento, Covalent grafting of phenylphosphonate groups onto layered silica derived from in-situ leached chrysotile fibers, J. Mater. Chem. 13 (2003) 304–307.
[14] U. Diaz, A. Cantin, A. Corma, Novel layered organic–inorganic hybrid materials with bridged silsesquioxanes as pillars, Chem. Mater 19 (2007) 3686–3693.
[15] R. Dey, C. Airoldi, Designed pendant chain covalently bonded to silica gel for cation removal, J. Hazard. Mater. 156 (2008) 95–101.
[16] A. Chaudhari, C.V. Kumar, Intercalation of proteins into α-zirconium phosphates: tuning the binding affinites with phosphate functions, Microporous Mesoporous Mater. 77 (2005) 175–187.
[17] P. Zhang, Y. Wang, G.S. Zhu, Z. Shi, Y.L. Liu, H.M. Yuan, W.Q. Pang, Hydrothermal synthesis and crystal structure of $Zn_4(PO_4)_2(HPO_4)2.0.5(C_{10}H_{28}N_4)\cdot 2H_2O$ a new layered zinc phosphate with 12-ring cavites, J. Solid State Chem. 154 (2000) 368–374.
[18] K.I. Ozoemena, T. Nyokong, D. Nkosi, I. Chambrier, M.J. Cook, Insights into the surface and redox properties of single-walled carbon nanotube–cobalt(II) tetra-aminophthalocyanine self-assembled on gold electrode, Eletrochim. Acta 52 (2007) 4132–4143.
[19] M. Ogawa, T. Ishii, N. Miyamoto, K. Kuroda, Intercalation of a cationic azobenzene into montmorillonite, Appl. Clay Sci. 22 (2003) 179–185.
[20] K. Goubitz, P. Capková, K. Melánová, W. Molleman, H. Schenk, Structure determination of two intercalated compounds $VOPO_4\cdot(CH_2)_4O$ and $VOPO_4\cdot OH–(CH_2)_2–O–(CH_2)_2–OH$; synchrotron power diffraction and molecular modeling, Acta Crystallogr. B 57 (2001) 178–183.
[21] P. Sharma, G. Singh, R. Tomar, Synthesis and characterization of an analogue of heulandite: Sorption and applications for thorium(IV), europium(III), samarium(II) and iron(II) recovery from aqueous waster, J. Colloid Interface Sci. 332 (2009) 298–308.
[22] I. Langmuir, The adsorption of gases on plane surfaces of glass, mica and platinum, J. Am. Chem. 57 (1918) 1361–1403.
[23] H.M.F. Freundlich, Über die adsorption in lösungen (adsoption in solution), Z. Phys. Chem. 57 (1906) 385–470.
[24] R. Sips, On the structure of a catalyst surface, J. Chem. Phys. 16 (1948) 490–495.

[25] A.R. Cestari, E.F.S. Vieira, G.S. Vieira, L.P. da Costa, A.M.G. Tavares, W. Loh, C. Airoldi, The removal of reactive dyes from aqueous solutions using chemically modified mesoporous silica in the presence of anionic surfactant—the temperature dependence and a thermodynamic multivariate analysis, J. Harzard. Mater 161 (2009) 307–316.
[26] Z. Aksu, F. Gönen, Biosorption of phenol by immobilized active sludge in a continuous packed bed: prediction of breakthrough curves, Process Biochem. 39 (2004) 599–613.
[27] M.V. Ernest, J.R.D. Whitley, Z. Ma, L.N.H. Wang, Effects of mass action equilibria on fixed-bed multicomponent ion-exchange dynamic, Ind. Eng. Chem. Res. 36 (1997) 212–226.
[28] D.L. Guerra, R.R. Viana, A. Airoldi, Thermochemical data for n-alkylmonoamine functionalization into lamellar silicate Al-kanemite, J. Chem. Thermodyn. 43 (2011) 69–74.
[29] W.J. Weber Jr., Adsorption, Physicochemical Process for Water Quality Control, Wiley, New York206–211.
[30] V.S.O. Ruiz, C. Airoldi, Thermochemical data for n-alkylmonoamine intercalation into crytalline lamellar zirconium phenylphosphonate, Thermochim. Acta 420 (2004) 73–78.
[31] H. Komine, Predicting hydraulic conductivity of sand–bentonite mixture backfill before and after swelling deformation for underground disposal of radioactive wastes, Eng. Geol. 114 (2010) 123–134.
[32] C.G. Pope, X-ray diffraction and the Bragg equation, J. Chem. Educ. 74 (1997) 129–135.
[33] S.A. Memon, R. Arsalan, S. Khan, T.Y. Lo, Utilization of Pakistan bentonite as partial replacement of cement in concrete, Constr. Build. Mater 30 (2012) 237–242.
[34] S. Xifang, L. Chum, W. Zhansheng, X. Xiaolin, R. Ling, Z. Hongsheng, Adsorption of protein from model wine solution by different bentonites, Chin. J. Chem. Eng. 15 (2007) 632–638.
[35] D. Shu-li, S. Yu-zhuang, Y. Cui-na, X. Bo-hui, Removal of copper from aqueous solutions by bentonite and the factors affecting it, J. Min. Sci. Technol. 19 (2009) 0489–0492.
[36] O. Altin, O.H. Ozbelge, T. Dogu, Effect of pH, flow rate and concentrations on the sorption of Pb and Cd on montmorillonite, J. Chem. Technol. Biotechnol. 74 (1999) 1131–1138.
[37] Y.S. Al-Degs, M.I. El-Barghouhi, A.H. El-Sheikh, G.M. Walker, Effect of solution pH, ionic strength, and temperature on adsorption behavior of reactive dyes on activated carbon, Dyes Pigments 77 (2008) 16–23.
[38] E. Malkoc, Y. Nuhoglu, M. Dundar, Adsorption of chromium(VI) on pomace – An olive oil industry waste: bath and column studies, J. Hazard. Mater. 138 (2006) 142–151.
[39] E. Zeynep, N.A. Filiz, Adsorption of reactive black 5 from an aqueous solution: equilibrium and kinetic studies, Desalination 194 (2006) 1–10.
[40] Y.S. Ho, G. McKay, Pseudo-isotherms for the sorption of cadmium ion onto tree fern, Process Biochem. 39 (2004) 759–763.
[41] N. Yeddou, A. Bensmaili, Kinetic models for the sorption of dye from aqueous solution by clay–wood sawdust mixture, Desalination 185 (2005) 499–508.
[42] D.L. Guerra, E.S. Mendonsa, R.A.R. Silva, W. Lara, Studies of Adsorption of pillarized and organofunctionalized smectite clay for Th^{4+} removal, J. Ceram. Sci. Technol. 3 (2012) 17–28.
[43] E. Malkoc, Y. Nuhoglu, Investigation of nickel(II) removal from aqueous solutions using tea factory waste, J. Hazard. Mater. B 127 (2005) 120–128.
[44] R.P. Han, J.H. Zhang, W.H. Zou, H.J. Xiao, J. Shi, H.M. Liu, Biosorption of copper(II) and lead(II) from aqueous solution by chaff in a fixed-bed column, J. Hazard. Mater. 133 (2006) 262–268.
[45] J. Goel, K. Kadirvelu, C. Rajagopal, V. Kumar Garg, Removal of lead(II) by adsorption using treated granular activated carbon: batch and column studies, J. Hazard. Mater. 125 (2005) 211–220.